



## Static Analysis and Design of a Flight Control with Oleopneumatic Centering for a Sidestick CPT/FO in A320 Simulators

Alexis Cordovés-García<sup>1\*</sup>, José Luís Palacios-Luna<sup>1</sup>, Raúl Vicente Paredes-Loor<sup>1</sup>,  
Alexis Cordovés-Rodríguez<sup>2</sup>, Leandro L. Lorente-Leyva<sup>3</sup>

<sup>1</sup> Faculty of Engineering Sciences and Industries, UTE University, Quito 170147, Ecuador

<sup>2</sup> CAD/CAM Studies Center, Faculty of Engineering, University of Holguin, Holguin 80100, Cuba

<sup>3</sup> SDAS Research Group, Ben Guerir 43150, Morocco

Corresponding Author Email: [alexis.cordoves@ute.edu.ec](mailto:alexis.cordoves@ute.edu.ec)

Copyright: ©2025 The authors. This article is published by IETA and is licensed under the CC BY 4.0 license (<http://creativecommons.org/licenses/by/4.0/>).

<https://doi.org/10.18280/mmep.120301>

### ABSTRACT

**Received:** 21 November 2024

**Revised:** 13 January 2025

**Accepted:** 20 January 2025

**Available online:** 31 March 2025

#### Keywords:

*A320 simulator, degrees of freedom, flight control design, oleo-pneumatic shock absorber, Sidestick CPT/FO, static simulation*

This study presents the design and validation of a Sidestick Captain/First Officer (CPT/FO) prototype with an oleo-pneumatic centering system as an enhancement for the FSTD A320 flight simulator, originally equipped with a conventional mechanical spring system. The objective was to improve the fidelity and response precision of the control system to provide a more realistic and efficient flight simulation experience. The methodology involved mechanical and structural design using SolidWorks, material selection (A36 Steel for the structure and 304 Stainless Steel for the control lever), and validation through static and numerical analyses to ensure structural integrity and system performance. The static analysis confirmed that the components operate within safe limits, and the integration of the oleo-pneumatic system provided a more stable and controlled damping response, closely replicating the behavior of the Airbus A320 Sidestick. Compared to traditional mechanical spring, electromechanical shock absorbers and hydraulic damper systems, the proposed design offers a smoother and more precise response while maintaining simplicity, low maintenance, and cost-efficiency. This innovation not only enhances the performance of the FSTD A320 simulator but also represents a scalable solution for other flight simulation models, contributing to more effective pilot training and opening opportunities for future improvements through advanced dynamic analysis.

## 1. INTRODUCTION

In the beginnings of aviation, flight command control was connected to mechanical drives, a system that persisted for many years. As airplanes needed to reach higher speeds and improve their control, electrical and hydraulic drives began to be used, which introduced improvements in the development and control of the forces to be applied in the command control system, thus the technology evolved towards the Fly-By-Wire system, giving way to piloting by electronic controls, this technology ended up being extended to many aviation models such as the Airbus A320 [1].

Sidestick-enabled aircraft allow the pilot's commands to be captured and transmitted, in the form of electrical signals, to the flight control computers. In some cases, there is no feedback to the pilot of the forces exerted by the air on the surfaces of the plane and the Sidestick is loaded with a spring that returns it to the neutral position [2].

Many commercial aircraft, such as Airbus, use passive side sticks that integrate with the electronic flight control system. These sticks include a servomechanism to provide force feedback and use strain gauges to determine the force applied to the side stick by the pilot [3].

The General Directorate of Civil Aviation (DGAC) in

Ecuador requires that career programs for the training of commercial pilots include hours of training with the use of flight simulators, with the best possible approximation to real flight conditions and the emerging technologies currently available [4-7].

Training in flight simulators has been assumed from several approaches. Villacís [8] created an interactive simulator supported by mathematical models based on the design of algorithms to simulate the flight of the aircraft from its physical behavior, being considered as a mass subjected to different forces, which allows reproducing the flight of an aircraft within simulation software.

Fernández-Villacañas Marín [9] incorporated new functionalities to combat aircraft flight simulation platforms, including the management of logistics support intelligence related to the simulated effort of hostile air operations and adverse weather conditions. On the other hand, Aronsson et al. [10] carried out a study of the main characteristics and design requirements of flight simulators. Yuksek and Inalhan [11] propose an innovative approach to flight control system design based on reinforcement learning. This method aims to optimize the transient response performance of an adaptive control system, achieving significant improvements in stability and adaptability to variable flight conditions.

Flight simulators have become essential tools in pilot training and the development of aeronautical control systems, offering safe and cost-effective environments for advanced testing and training [12-16]. The integration of advanced technologies into the electromechanical design of flight controls has achieved significant milestones in precision and dynamic response, enhancing both user experience and skill transfer to real-world flight scenarios [17-21]. Additionally, recent research highlights the impact of virtual and augmented reality in creating more immersive and adaptive simulation environments, capable of replicating flight conditions with a high degree of realism [22, 23]. Simultaneously, the use of advanced materials and the adoption of additive manufacturing technologies, such as 3D printing, have revolutionized the production of electromechanical components [24], significantly reducing manufacturing and maintenance costs. These advancements underscore the central role of flight simulators and electromechanical design in the transformation and modernization of contemporary aviation.

From a training perspective, simulators are designed to develop knowledge and skills that allow correct decision-making in adverse situations, trained in a combined learning environment [25], if possible, in multi-platform advanced learning systems [26], taking advantage of modeling and simulation (M&S) capabilities to support operational testing and systems analysis [27].

This research focuses on the flight control of the Airbus A320, taking advantage of the data available from this aircraft, with the aim of developing a virtual prototype of the CPT/FO Sidestick incorporating an oleopneumatic system. This design seeks to improve the sensitivity and fidelity of the FSTD A320 flight simulator, currently based on conventional mechanical springs that offer a static and limited response. Mechanical springs generate a constant resistance, independent of the applied force, which produces a rigid and unrealistic control sensation. This lack of variability affects the simulator's ability to accurately replicate the dynamic conditions faced by the pilot during complex maneuvers.

A flight control with oleo-pneumatic centering was designed, using SolidWorks CAD Software, considering the dimensional description and functional characteristics of the Airbus A320 flight control, ensuring the magnitude of the displacements and degrees of freedom of its Sidestick device.

The static analysis of the prototype components was carried out to verify that the design of the structure satisfies the geometric, dimensional and functional requirements; according to the request to which its component elements are subjected.

In order to achieve a full integration of the new Sidestick into the FSTD A320 simulator, it is necessary to implement specific hardware and software interfaces. On the hardware side, the installation of position and force sensors is required, together with an electronic interface that converts physical signals into digital data compatible with the simulator. On the software side, it is essential to develop and integrate specific drivers that manage communication between the Sidestick and the simulator. This encompasses data acquisition systems, modelling and simulation of dynamic behaviour, as well as the implementation of communication protocols that ensure the correct transmission of information, thus ensuring precise and realistic operation.

## 2. MATERIALS AND METHODS

This new design will be composed of oleo-pneumatic dampers with self-centering to regulate the point of origin. The design includes pieces anchored to the frame that provide degrees of freedom to the system. The selection of dampers must guarantee their specific resistance and the force of resistance to movement.

The required damping coefficient, distances and forces applied to the parts of the system were determined. Through a static analysis of each model obtained in SolidWorks, the value of the stresses and deformations present in each of the parts of the system was determined, by numerical methods, to validate the capacity of the device to resist the stresses present during its operation. Figures 1 and 2 show the functional and non-functional requirements of the product.

A36 steel was selected as the material for the basic and supporting structural elements of the Sidestick, given the moderate load conditions that act in a flight simulator, significantly lower than those in real aeronautical environments. This makes it suitable to withstand these loads without oversizing the design, ensuring a favorable balance between mechanical strength, durability, ease of manufacture and costs. For the control stick, 304 stainless steel was chosen, a choice justified by its excellent mechanical properties, corrosion resistance and its adequate response to continuous use, meeting the functional and structural requirements of the FSTD A320 flight simulator.

A fixed base was designed (see Figure 3), with the main function of anchoring the general system of degrees of freedom to the frame of the box, using pins located perpendicular to the exterior faces, the same hole that will be used to assemble the internal parts of the system.

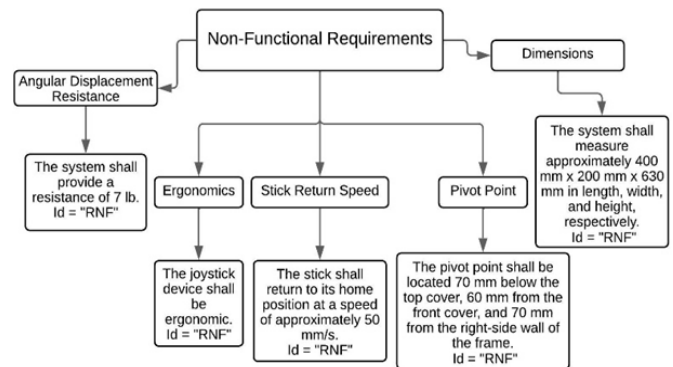


Figure 1. Non-functional requirements diagram

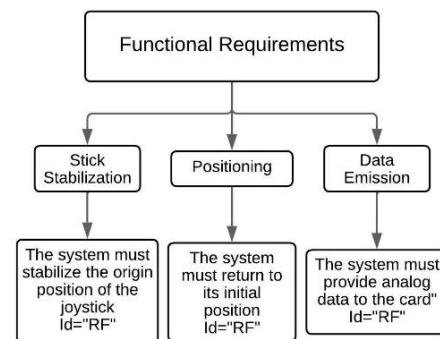
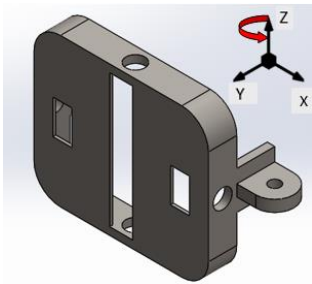


Figure 2. Functional requirements diagram



**Figure 3.** External part of the degrees of freedom mobility system



**Figure 4.** Intermediate piece of the degrees of freedom mobility system

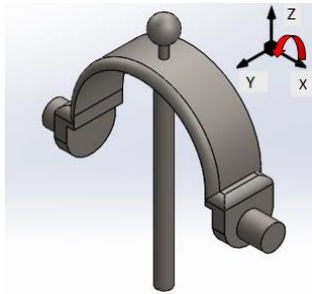


**Figure 5.** Internal part of the degrees of freedom mobility system

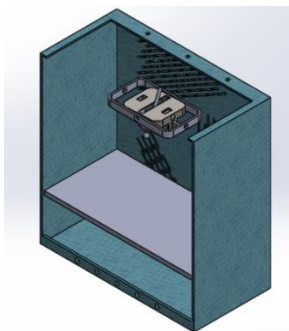


**Figure 6.** Model of the box and the degrees of freedom mobility system

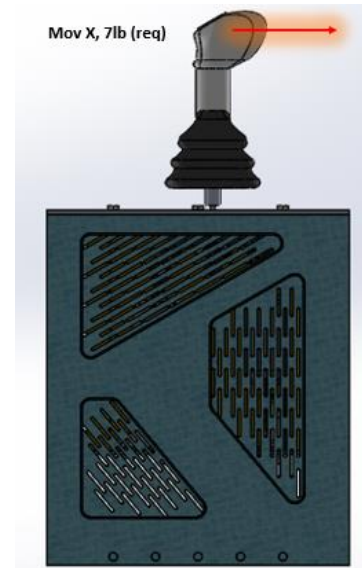
Figure 4 shows the intermediate piece of the degrees of freedom mobility system, which fulfills the main function of granting the first degree of freedom in the movement of the lever through rotation in the "z" axis through the two central holes located on the front and rear faces in the working position. In addition, this piece has the required anchors for the external couplings of the dampers.

Figure 5 shows the internal part of the degrees of freedom mobility system, which has the main function of granting the second degree of freedom in the movement of the lever,

through its rotation around the "x" axis with pins exposed on the faces right and left sides. This piece also has the spherical coupling for the end of the damper and the cylindrical shaft that connects to the lever.

The design of the frame where the entire system was located (see Figure 6) was made by considering the original measurements of the Sidestick from the Latin American Aeronautics – Vortex Airspace company. Which ensures minor changes to the general structure of the Sidestick.

Figure 7 depicts the force vector applied by the pilot during a maneuver and that requires to be reversed by the damping through self-centering. This determines a specific damping resistance of 7 lb, according to the Sidestick technical sheet, and the standard of the Airbus A320 commercial aircraft.



**Figure 7.** Indication of the force vector exerted by the pilot

## 2.1 Damping factor calculation

The damping factor ( $\zeta$ ) measures the level of energy dissipation of the system compared to the critical damping, and indicates the response of the system to disturbances and is determined by the equation:

$$\xi = \frac{c}{Cc} \quad (1)$$

where,

$c$  = linear damping coefficient

$Cc$  = critical damping coefficient

Every mechanical damping device has a damping constant ( $c$ ) that governs the behavior of the mechanism when an external force is exerted on it and that can be determined from the technical data of the selected damper and the operating conditions. The critical damping ( $Cc$ ) is the value that allows the system to return to equilibrium without oscillation and in the shortest possible time.

Next, the values of the actual linear damping coefficient and the  $Cc$  value will be determined.

### 2.1.1 Calculation of the damping coefficient

In this case, the 89U076214TT shock absorber from Industrial Gas Springs, Inc. was selected, whose data are indicated in Table 1, which respond to the dimensional and operational requirements of the Sidestick CPT/FO.

**Table 1.** Damper data sheet

Product Details	
Stock Number	89U076214TT
Product type	Compression Gas Spring
Rod Ø	8 mm (0.31 in)
Body Ø	18 mm (0.71 in)
Stroke	76.20 mm (3 in)
Shoulder Length	217.93 mm (8.58 in)
Rod End	Threaded
Body End	Threaded
Rod Material	Black Nitride Carbon Steel
Body Material	Carbon Steel W/Black Epoxy Paint
Rod Position on Model (0,00-3,00 in)	3.00
Force Range (lbs)	N/A
Damping	N/A
K Factor	1.3
Net Weight	5.8 oz (0.1644 kg)
Ball Socket Diameter	N/A
Damping Type	Compression
Dampening Specification	1 second / 1 in @ 20 lbs. load
Compressed Shoulder Length	141.73 mm (5.58 in)

Source: Industrial Gas Springs, Inc.

Assuming that the damping specification behaves linearly for small variations in force values, it was determined that to damp a force value of 10 lbf (44.482 N), a dampening specification of half a second per inch, from the relation:

$$\frac{1s}{1in} \rightarrow \frac{X}{20lbf} \rightarrow \frac{X}{10lbf} \quad (2)$$

Which corresponds to a value of  $0.01969 \frac{s}{mm}$  when expressing the time in “s” and the distance traveled, in mm. The inverse of this value corresponds to the magnitude of the speed, expressed in mm/s, at which the damper stem expands and compresses, as follows:

$$V = \left[0.01969 \frac{s}{mm}\right]^{-1} = 50.8 \frac{mm}{s} \quad (3)$$

From the value obtained of the speed and the force that the damper must resist, its linear damping constant is determined, which is a parameter that indicates its capacity to dissipate the energy absorbed by the rod, and is calculated using the expression:

$$F = c * v \quad (4)$$

where,

*F*: damper resistant force

*c*: real linear damping constant

*v*: relative velocity between association points

Therefore:

$$c = \frac{F}{v} = \frac{44.482N}{50.8 \frac{mm}{s}} = 0.88 \frac{N*s}{mm}$$

### 2.1.2 Calculation of Cc

*Cc* is calculated by the expression:

$$Cc = 2\sqrt{k.m} \quad (5)$$

where,

*k*: shock absorber stiffness constant (see Table 1)

*m*: effective mass of the shock absorber (see Table 1)

The stiffness constant (*k*) for a system such as the Sidestick CPT/FO with oleopneumatic shock absorber, represents the relationship between the applied force and the displacement of the rod. The critical damping according to Eq. (5) would be:

$$Cc = 2\sqrt{1.3 \times 0.1644} = 0.925 \text{ N s/mm}$$

Finally, by substituting the values obtained from the coefficients (*c*) and (*Cc*) in equation Eq. (1), the value of the damping factor ( $\xi$ ) is obtained.

$$\xi = \frac{0.88}{0.925} = 0.95$$

### 2.2 Calculation of distances and travel of the damper stem

From the technical specifications of the oleo-pneumatic shock absorber (Table 1) and the extreme positions of the rod shown in Figure 8, it can be deduced that the piston rod will have a maximum travel in extension of 217.93 mm and in compression a minimum travel of 141.73 mm. So the actual working stroke of the stem is 76.2 mm. The cylinder diameter is 18 mm and the stem diameter is 8 mm, the dimensions of the end couplings are not considered.

The average piston rod travel value (38.1 mm) is half of the total piston rod travel (76.2 mm). When this is located in its mid-travel position, it will have the ability to compress and expand when the required force is applied.

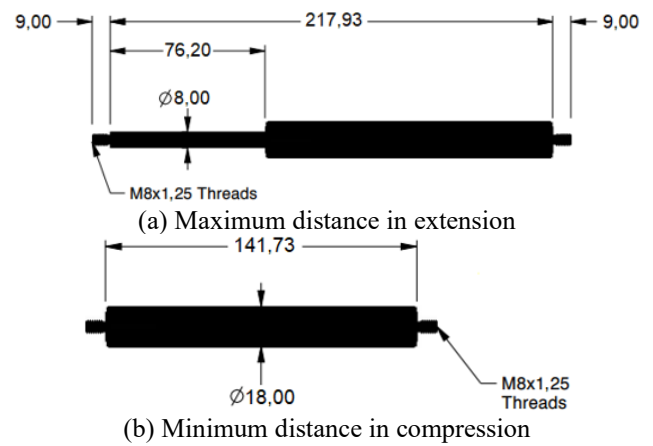


**Figure 8.** Damper piston rod travel diagram

From the value obtained in the average stroke and the value of the distance of the damper with the piston rod in extension, the calculation of the variable “a” was carried out (see Figure 8).

$$\begin{aligned} a &= \text{shoulder length-average stroke} \\ a &= 217.93 \text{ mm} - 38.1 \text{ mm} \\ a &= 179.83 \text{ mm} \end{aligned} \quad (6)$$

Since a right triangle is formed by locating each damper with respect to its base inside the Sidestick box, a value for the installation angle  $\beta_{inst}$  de  $40^\circ$  was set, which will be modified during Sidestick operation in expansion or compression (see Figure 9).

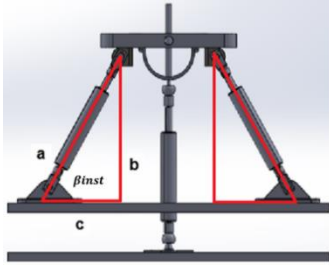


**Figure 9.** Scheme for geometric calculations of the location of the dampers

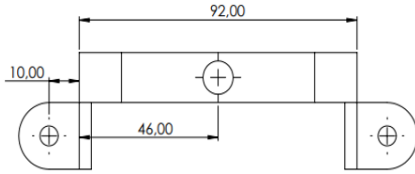


**Figure 10.** Dimensions of the intermediate piece of the degrees of freedom mobility system

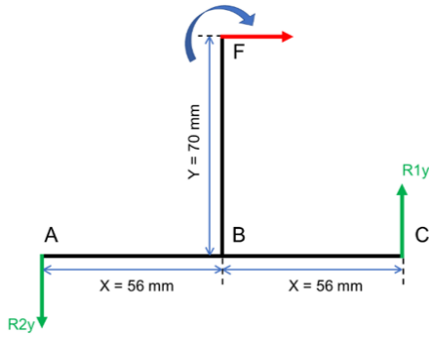


**Figure 11.** Static diagram of the rigid body

The value of leg “b” was determined from the trigonometric sine function of  $\beta_{inst}$ , knowing the value of the hypotenuse “a”. That is the distance to set the position of the damper in the Y axis and its value is 115.59 mm. Similarly, by applying the trigonometric cosine function of  $\beta_{inst}$ , knowing the value of the hypotenuse “a”, the value of leg “c” was determined, and it was assumed as the location distance of the damper on the X axis and its value is 137.757 mm.

Figure 10 shows the intermediate piece of the mobility system of degrees of freedom to which the respective moment calculations were carried out, in order to know what force the shock absorbers exert when applying the required force at the pivot point.

The rigid body diagram of the intermediate piece of the mobility system of degrees of freedom was made (see Figure 11), in which the forces and reactions involved are indicated with their respective distances. The clockwise direction was assumed as positive for the calculation of moments.

$$\begin{aligned}
 M &= F * d \\
 F(70 \text{ mm}) - R_{1y}(56 \text{ mm}) - R_{2y}(56 \text{ mm}) &= 0 \\
 \text{for } R &= R_{1y} = R_{2y} \\
 \text{then: } F(70 \text{ mm}) - 2[R(56 \text{ mm})] &= 0 \\
 R &= \frac{-F(0.070 \text{ m})}{-0.112 \text{ m}} \\
 R &= \frac{(-31.1374 \text{ N})(0.070 \text{ m})}{-0.112 \text{ m}} \\
 R &= 19.46 \text{ N}
 \end{aligned} \tag{7}$$

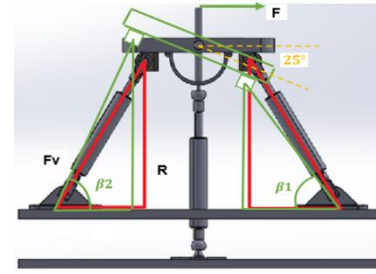


**Figure 12.** Scheme for calculating the real force on the piston rod

Using trigonometric equations, the right triangle was solved with the two data presented. For this, the sine operation of the beta installation angle was used to obtain the value of the force of the piston rod (see Figure 12).

Data:

$$\beta_{inst} = 40^\circ; R = 19.46 \text{ N}$$

Calculation of the force on the piston rod ( $F_v$ ).

$$\begin{aligned}
 \sin \beta_{inst} &= \frac{R}{F_v} \\
 F_v &= \frac{19.46 \text{ N}}{\sin 40^\circ}
 \end{aligned} \tag{8}$$

where,

$$\begin{aligned}
 F_v &< \text{maximum strength} \\
 F_v &= 30.274 \text{ N} \\
 30.274 \text{ N} &< 44.482 \text{ N}
 \end{aligned}$$

The calculation of the variation of the piston rod force, according to the installation angle was carried out, based on the diagram made in Figure 12,  $\beta_1$  is the smallest possible angle of the damper and  $\beta_2$  is the largest possible angle of the damper, the values of these angles were taken from the assembly made in SolidWorks, where:

$$\beta_1 = 33.73^\circ; \beta_2 = 46.27^\circ$$

Calculation of the maximum outside of the piston rod.

$$\begin{aligned}
 F_v \text{ max} &= \frac{R}{\sin \beta_1} \\
 F_v \text{ max} &= \frac{19.46 \text{ N}}{\sin 33.73^\circ}
 \end{aligned} \tag{9}$$

where,

$$\begin{aligned}
 F_v \text{ max} &< \text{maximum strength} \\
 F_v \text{ max} &= 35.045 \text{ N} \\
 35.045 \text{ N} &< 44.482 \text{ N}
 \end{aligned}$$

Calculation of the minimum outside of the piston rod.

$$\begin{aligned}
 F_v \text{ min} &= \frac{R}{\sin \beta_2} \\
 F_v \text{ min} &= \frac{19.46 \text{ N}}{\sin 46.27^\circ} \\
 F_v \text{ min} &= 26.930 \text{ N}
 \end{aligned} \tag{10}$$

The choice of the commercial damper made is correct, since the selected damper delivers, by design, up to a force of 44.482 N, and the maximum force of the stem is 35.045 N.

### 3. RESULTS AND DISCUSSION

#### 3.1 Static analysis of each part of the system

Once the geometric models of each component element of the oleo-pneumatic system of the Sidestick CPT/FO device were generated, the static analysis of each part was carried out with the help of the SolidWorks static simulation module. The value of the stresses, displacements, unitary deformations and reaction forces of the modeled parts was determined, in order to evaluate the behavior of the element and guarantee the operation of the mechanism.

The boundary conditions and applied loads were selected to faithfully replicate the operating environment of the CPT/FO Sidestick. Reasonable simplifications were considered, such as the absence of friction and the application of static loads, justified by the need to obtain representative results in a static simulation environment.

During the application of the loads, a point force was applied to the upper end of the Sidestick, representing the pilot's action during a maneuver. The force was 44.482 N (7 lb), a value calculated according to the technical specifications of the Airbus A320 Sidestick.

Figure 13 indicates the static nodal stress analysis of the external piece on a deformation scale with Von Mises failure criteria, where the maximum stress limit acting on the piece can be observed.

Figure 14 illustrates the result of the analysis of the static unitary strain suffered by the external piece, on an equivalent strain scale.

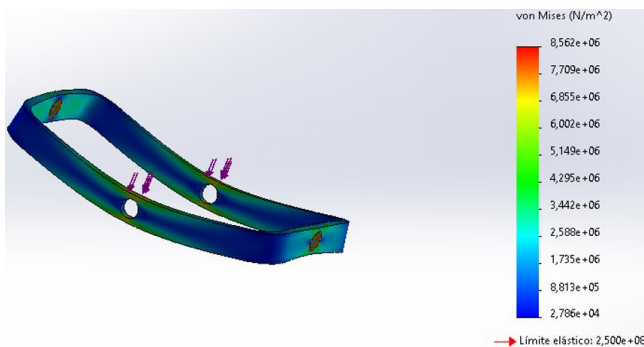


Figure 13. Static analysis external part nodal stress

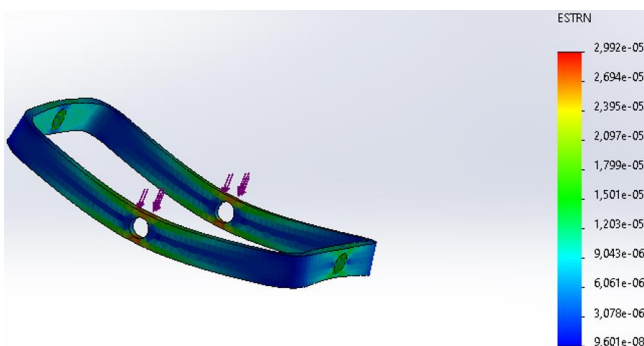


Figure 14. Static unitary strain, external part

The external part serves the function of anchoring the system to the frame and at the same time supporting the remaining elements of the system, which suggests that it is one of the elements with the greatest demands during the operation of the Sidestick. In this way, the support given by the connection of pins in both central holes on the most distant faces of the part is defined as a boundary condition. In addition, the load transmitted to the part is delimited, through the connection by pins with the intermediate part of the mobility system of degrees of freedom.

In the simulation, a maximum stress of  $8,562 \times 10^6$  Pa is reached, much lower than the elastic limit of the material  $2,500 \times 10^8$  Pa, so the deformations that occur will be found in the elastic zone of the material.

Regarding the result of the analysis of the static unitary deformation suffered by the external piece, with a value of  $2,992 \times 10^{-5}$  mm (Figure 14), it is concluded that it is a small deformation that does not affect the operation of the system.

Next, the static analysis was carried out on the intermediate piece of the degrees of freedom mobility system, when the stress was determined according to the Von Mises failure criterion, in Pa (see Figure 15).

In this case, the boundary condition is identified as the fastening of the intermediate piece of the freedom degree mobility system to the external piece, using pins; and the load would be applied to the lateral supports of the external couplings to the shock absorbers.

Figure 16 shows the result, at ESTRN scale, of the analysis of the static unitary deformation of the intermediate piece of the mobility system of degrees of freedom when absorbing the acting loads.

The main function of the intermediate piece is to provide the device with the first degree of freedom in movement in the X axis of the lever. For the study, the fixings were established and the forces were applied to their pin supports and anchors for the gate couplings.

The Von Mises stress value reached by the piece in the static analysis is  $4,736 \times 10^6$  Pa (see Figure 15), lower than the elastic limit of the material of  $2,500 \times 10^8$  Pa.

The static unit strain analysis of the intermediate piece shows a deformation value of  $1,748 \times 10^{-5}$  mm that does not affect the operation of the piece.

Figure 17 shows the static nodal stress analysis carried out on the internal part according to the Von Mises failure criterion.

For this analysis, the boundary restriction is specified as the support provided by the connection of the cylindrical ends exposed on the right and left side faces of the piece, with the intermediate piece of the degree of freedom mobility system, the load would be applied through the axis of the piece.

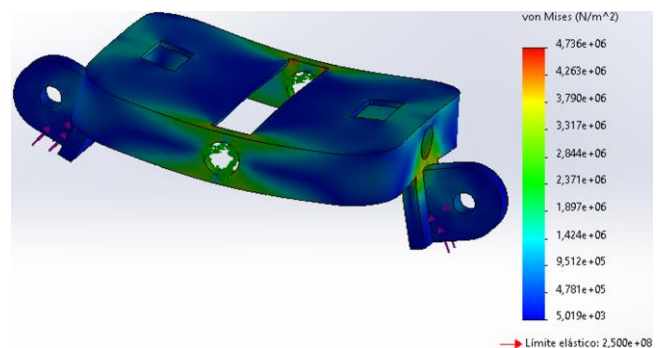


Figure 15. Static analysis nodal stress intermediate piece

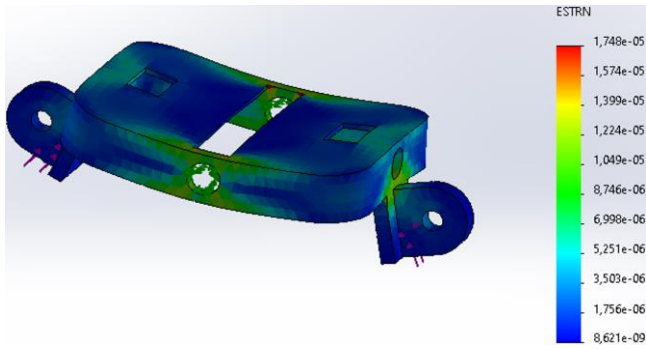


Figure 16. Static unitary strain, intermediate piece

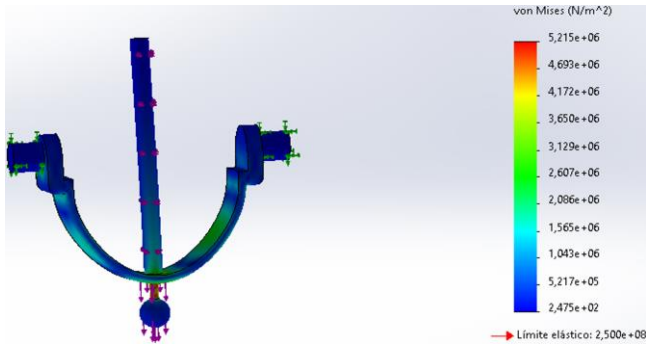


Figure 17. Static analysis nodal stress, internal piece

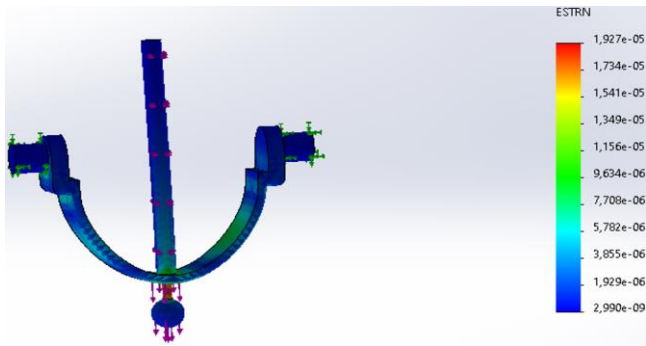


Figure 18. Static unitary strain, internal piece

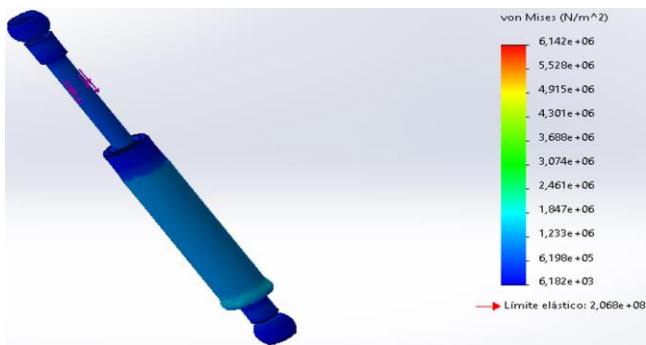


Figure 19. Static analysis nodal stress of the damper

Von Mises failure criterion of  $5,215 \times 10^6$  Pa (see Figure 17), lower than the elastic limit of the material of  $2,500 \times 10^8$  Pa.

On the other hand, the deformation analysis shows a value of  $1,927 \times 10^{-5}$  mm (see Figure 18), a value that does not affect the operation of the internal part within the system.

Figure 19 shows the static nodal stress analysis carried out on the damper, according to the Von Mises failure criterion, in Pa.

As has been said, the oleo-pneumatic damper system fulfills the function of self-centering the Sidestick by ceasing the action of the force exerted by the pilot during a maneuver. The force was applied at the end coupling of the piston rod and clamping at the end coupling of the cylinder.

Besides, Figure 20 illustrates the result, at an equivalent strain scale, of the analysis of the static unitary deformation of the damper.

As a result, a nodal stress was obtained, according to the Von Mises failure criterion, of  $6,142 \times 10^6$  Pa (Figure 19), lower than the elastic limit of the material of  $2,500 \times 10^8$  Pa.

The analysis of static unitary strain, at an equivalent strain scale, shows a value of  $1,964 \times 10^{-5}$  mm, a value that does not affect the operation of the damping in the degrees of freedom mobility system (Figure 20).

In a general analysis of the behavior of the degrees of freedom mobility system, in all cases, nodal stress values lower than the elastic limit of the material were recorded.

The maximum value obtained for nodal stress,  $8,562 \times 10^6$  Pa, corresponds, as expected, to the external part, due to its function as a support part. Likewise, the piece recorded the maximum static unitary strain of  $2,992 \times 10^{-5}$  mm.

The robustness of the shape of the intermediate piece allowed it to register the minimum values of nodal stress,  $4,736 \times 10^6$  Pa, and static unitary deformation,  $1,748 \times 10^{-5}$  mm.

Static analysis showed that the components of the oleopneumatic Sidestick operate within safe margins, with minimal deformations that ensure structural stability without compromising the precision of the movement. The nodal stress values remained below the elastic limit of the structural element's material (A36 steel), guaranteeing a linear and predictable response to the applied loads, an essential condition to accurately replicate the behaviour of the Airbus A320 Sidestick.

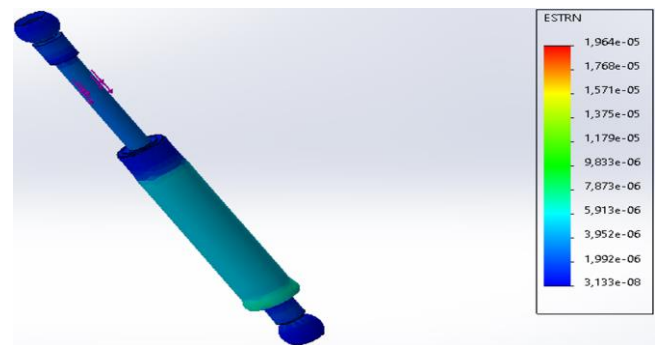


Figure 20. Static unitary strain of the damper

Figure 18 shows the equivalent deformation result of the static unitary deformation analysis of the internal part, in the degrees of freedom mobility system.

To carry out the static analysis of the internal part, the forces acting on the axis were applied, the fastenings were selected in the supports that are assembled to the intermediate piece and in the spherical coupling for the end of the central damper of the system. Thus, a nodal stress is reached according to the

### 3.2 Analysis of the influence of the damping coefficient and the damping factor

Regarding the behavior of the system to dampen the force exerted by the pilot when operating the Sidestick and allowing the lever to return to the neutral position, it can be stated that a value of the real linear damping coefficient (c) of 0.88

N.s/mm, indicates an adequate relationship between the applied force and the speed of movement of the rod, ensuring an adequate balance between energy dissipation and response capacity, with a controlled and rapid return of the lever to its neutral position, a crucial aspect in situations that require rapid maneuvers.

A higher value of the coefficient (c) would increase the stability of the system, but also the resistance to movement, making the movement of the rod slower, affecting the pilot's perception of control and could compromise the response speed.

The damping factor  $\xi=0.95$  indicates that the system is slightly underdamped, but very close to critical damping. This behavior implies that the system:

- Responds quickly to disturbances.
- Returns to equilibrium without perceptible oscillations.

•It offers stability and precision.

These are ideal conditions for a flight control system such as the Sidestick CPT/FO.

This balance between response speed and stability confirms that the damper selection is appropriate for the proposed design, contributing to the fidelity and safety of the flight simulator.

### 3.3 Comparison of the findings of the oleopneumatic damping system against other existing technologies or solutions

When comparing the findings of the oleo-pneumatic damping system versus other existing technologies or solutions used in simulators, the significant differences presented in Table 2 stand out.

**Table 2.** Comparative analysis of oleo-pneumatic and other damping systems

Other Technological Systems	Operating Characteristics	Limitations/Advantages	Behavior Compared to Oleo-Pneumatic Systems
Conventional Mechanical Spring	They use mechanical springs for centering the Sidestick	Less precise and less realistic response due to the absence of adjustable damping control	The oleopneumatic system offers a smoother and more controlled return, improving the pilot's feeling, as in a real system.
Electromechanical Shock Absorbers	Use electric motors and sensors to generate haptic feedback	Dynamic control of the applied force, allowing adjustment of resistance in real time	Despite of not allowing dynamic control of forces. The oleopneumatic system stands out for its mechanical simplicity, lower maintenance and reduced cost.
Traditional Hydraulic Shock Absorbers	Use hydraulic fluids to dissipate energy	Greater complexity, risk of leaks and maintenance costs	Oleo-pneumatic design combines damping efficiency with a more compact and reliable system.

## 4. CONCLUSIONS

This study presents the design and validation of a CPT/FO Sidestick prototype with oleopneumatic centering system, developed as an upgrade for the FSTD A320 flight simulator previously equipped with a conventional mechanical spring system. The new design seeks to overcome the limitations of fidelity and precision in response, providing more realistic and efficient control. The selection of A36 Steel for the structure and 304 Stainless Steel for the joystick ensures high mechanical strength, durability and a finish suitable for continuous use.

The results of the static analysis confirmed that the Sidestick components operate within safe margins, demonstrating the structural robustness of the design. The integration of the oleopneumatic system optimizes the dynamic response, providing a stable and controlled damping behavior, similar to that of the Airbus A320 Sidestick. The combination of numerical simulations and theoretical analysis validates the feasibility and effectiveness of the proposed design.

Compared to traditional mechanical spring systems and hydraulic dampers, the developed Sidestick offers a smoother and more stable response, avoiding oscillations and improving control precision. Furthermore, compared to electromechanical solutions, it stands out for its simplicity, low maintenance and reduced cost, while maintaining high standards of safety and efficiency.

This design not only improves the performance of the FSTD A320 simulator, but also represents an adaptable and scalable solution for other simulator models. In addition, it opens up new opportunities for future research, such as carrying out a detailed dynamic analysis, which will be addressed in future studies.

## REFERENCES

- [1] Schmitt, V.R., Jenney, G.D., Morris, J.W. (1998). Fly-by-Wire. SAE International.
- [2] Espinosa Moyano, R. (2015). Manual del Piloto de Ultraligero. ULM Multiejes de Ala fija. ULM Por Desplazamiento del Centro de Gravedad (DCG). Ediciones Paraninfo, SA.
- [3] Farwick, K. (2017). ActivSense sidestick: A force sensing and force feedback joystick. California Polytechnic State University.
- [4] Rico, L.C.V., Rodríguez, E.J.A., Melo, J.A.T. (2018). Simuladores de vuelo: Una revisión. Ciencia y Poder Aéreo, 13(2): 138-149. <https://doi.org/10.18667/cienciaypoderaereo.606>
- [5] Martín, M.A.G., Martín, P.P.G., Calero, P.A.G. (2007). Aprendizaje activo en simulaciones interactivas. Inteligencia Artificial. Revista Iberoamericana de Inteligencia Artificial, 11(33): 25-36.
- [6] Wallace, J. W., Hu, Z., Carroll, D.A. (2020). Augmented reality for immersive and tactile flight simulation. IEEE Aerospace and Electronic Systems Magazine, 35(12): 6-14. <https://doi.org/10.1109/MAES.2020.3002000>
- [7] Ross, G., Gilbey, A. (2023). Extended reality (xR) flight simulators as an adjunct to traditional flight training methods: A scoping review. CEAS Aeronautical Journal, 14(4): 799-815. <https://doi.org/10.1007/s13272-023-00688-5>
- [8] Villacís, C., Romero, F., Navarrete, M., Fuertes, W., et al. (2018). Mathematical models applied in the design of a flight simulator for military training. In Developments and Advances in Defense and Security: Proceedings of

- the Multidisciplinary International Conference of Research Applied to Defense and Security, Salinas, Ecuador, pp. 43-57. [https://doi.org/10.1007/978-3-319-78605-6\\_4](https://doi.org/10.1007/978-3-319-78605-6_4)
- [9] Fernández-Villacañas Marín, M.A. (2019). The transformation of the modelling & simulation of systems for the training of the CAF: Design requirements and new functionalities. In *Applied Technologies: First International Conference, ICAT 2019, Quito, Ecuador*, pp. 325-339. [https://doi.org/10.1007/978-3-030-42517-3\\_25](https://doi.org/10.1007/978-3-030-42517-3_25)
- [10] Aronsson, S., Artman, H., Lindquist, S., Mitchell, M., et al. (2019). Supporting after action review in simulator mission training: Co-creating visualization concepts for training of fast-jet fighter pilots. *The Journal of Defense Modeling and Simulation*, 16(3): 219-231. [10.1177/1548512918823296](https://doi.org/10.1177/1548512918823296)
- [11] Yuksek, B., Inalhan, G. (2021). Reinforcement learning based closed-loop reference model adaptive flight control system design. *International Journal of Adaptive Control and Signal Processing*, 35(3): 420-440. <https://doi.org/10.1002/acs.3181>
- [12] Kozuba, J., Śladkowski, A. (2021). Simulators as an essential tool for shaping the competence of the aviation personnel. In *Research Anthology on Reliability and Safety in Aviation Systems, Spacecraft, and Air Transport*, pp. 487-529. <https://doi.org/10.4018/978-1-7998-5357-2.ch019>
- [13] Källström, J., Granlund, R., Heintz, F. (2022). Design of simulation-based pilot training systems using machine learning agents. *The Aeronautical Journal*, 126(1300): 907-931. <https://doi.org/10.1017/aer.2022.8>
- [14] Dinçer, N. (2023). Elevating aviation education: A comprehensive examination of technology's role in modern flight training. *Journal of Aviation*, 7(2): 317-323. <https://doi.org/10.30518/jav.1279718>
- [15] Vidakovic, J., Lazarevic, M., Kvrđic, V., Vasovic Maksimovic, I., Rakic, A. (2021). Flight simulation training devices: Application, classification, and research. *International Journal of Aeronautical and Space Sciences*, 22(4): 874-885. <https://doi.org/10.1007/s42405-021-00358-y>
- [16] Cross, J., Boag-Hodgson, C., Ryley, T., Mavin, T.J., Potter, L.E. (2022). Using extended reality in flight simulators: A literature review. *IEEE Transactions on Visualization and Computer Graphics*, 29(9): 3961-3975. <https://doi.org/10.1109/TVCG.2022.3173921>
- [17] Fu, J., Maré, J.C., Fu, Y. (2017). Modelling and simulation of flight control electromechanical actuators with special focus on model architecting, multidisciplinary effects and power flows. *Chinese Journal of Aeronautics*, 30(1): 47-65. <https://doi.org/10.1016/j.cja.2016.07.006>
- [18] Jian, F.U., Jean-Charles, M.A.R.E., Liming, Y.U., Yongling, F.U. (2018). Multi-level virtual prototyping of electromechanical actuation system for more electric aircraft. *Chinese Journal of Aeronautics*, 31(5): 892-913. <https://doi.org/10.1016/j.cja.2017.12.009>
- [19] Pollack, T., Looye, G., Van der Linden, F. (2019). Design and flight testing of flight control laws integrating incremental nonlinear dynamic inversion and servo current control. In *AIAA Scitech 2019 Forum, San Diego, California*, pp. 0130. <https://doi.org/10.2514/6.2019-0130>
- [20] Bertolino, A.C., De Martin, A., Jacazio, G., Sorli, M. (2023). Design and preliminary performance assessment of a PHM system for electromechanical flight control actuators. *Aerospace*, 10(4): 335. <https://doi.org/10.3390/aerospace10040335>
- [21] Maré, J.C. (2020). Practical considerations in the modelling and simulation of electromechanical actuators. *Actuators*, 9(4): 94. <https://doi.org/10.3390/act9040094>
- [22] King, G., Carmody, K., Deaton, J. (2023). The influence of new realities: How virtual, augmented, and mixed reality advance training methods in aviation. In *Human Factors in Simulation and Training*, pp. 317-330. <https://doi.org/10.1201/9781003401353>
- [23] Nwobodo, O.J., Kuaban, G.S., Kukuczka, T., Wereszczyński, K., Cyran, K. (2024). Analysis of marker and slam-based tracking for advanced augmented reality (AR)-based flight simulation. In *Computational Science - ICCS 2024: 24th International Conference, Malaga, Spain*, pp. 208-222. [https://doi.org/10.1007/978-3-031-63783-4\\_16](https://doi.org/10.1007/978-3-031-63783-4_16)
- [24] Sun, W., Zhao, N. (2024). Vertical take-off and landing unmanned aerial vehicle design based on foam 3D printing technology. *IEEE Access*, 12: 184560-184582. <https://doi.org/10.1109/ACCESS.2024.3506597>
- [25] Ramírez, R. (2016). Flight simulator training for air force pilots in a blended learning environment. Master dissertation, Tecnológico de Monterrey, Mexico.
- [26] Freeman, J., Zachary, W. (2018). Intelligent tutoring for team training: Lessons learned from US military research. In *Building Intelligent Tutoring Systems for Teams: What Matters*, pp. 215-245. <https://doi.org/10.1108/S1534-085620180000019013>
- [27] Hill, R.R., Tolk, A., Hodson, D.D., Millar, J.R. (2018). Open challenges in building combat simulation systems to support test, analysis and training. In *2018 Winter Simulation Conference (WSC), Gothenburg, Sweden*, pp. 3730-3741. <https://doi.org/10.1109/WSC.2018.8632233>